American Mineralogist, Volume 83, pages 700–711, 1998

Oxygen diffusion in rutile from 750 to 1000 °C and 0.1 to 1000 MPa

D.K. Moore,[1,*] D.J. Cherniak,[2] and E.B. Watson[2]

[1]American Geophysical Union, 2000 Florida Avenue, N.W., Washington, D.C. 20009, U.S.A.
[2]Department of Earth and Environmental Sciences, Rensselaer Polytechnic Institute, Troy, New York 12180, U.S.A.

Abstract

Oxygen self-diffusion in rutile was studied in synthetic and natural samples over the temperature range 750 to 1000 °C and the pressure range 0.1 to 1000 MPa using an ^{18}O-enriched source. Most experiments investigated the dependence of D on temperature, water pressure, crystallographic direction, and experiment duration. A few experiments investigated the dependence of D on f_{O_2} and confining pressure. The uptake profiles of ^{18}O in experimental products were measured by nuclear reaction analysis using the reaction $^{18}O(p,\alpha)^{15}N$.

Two mechanisms are responsible for O diffusion in rutile, and one is faster than the other by about an order of magnitude. O that diffuses by the faster mechanism is described by the diffusion law:

$$D(\|c) = 4.7 \times 10^{-7} \exp(-258 \pm 22 \times 10^3/RT)\ D_0 \text{ in m}^2/\text{s};\quad E_A \text{ in J/mol};\quad T \text{ in K.}$$

Diffusion by the slower mechanism is described by this law:

$$D(\|c) = 5.9 \times 10^{-5} \exp(-330 \pm 15 \times 10^3/RT)\ D_0 \text{ in m}^2/\text{s};\quad E_A \text{ in J/mol};\quad T \text{ in K.}$$

Oxygen fugacity in itself does not affect D at fugacities between 1 atm and Ni-NiO. However, the presence or absence of water during reduction does affect the diffusion behavior. When water is absent during rutile growth and/or subsequent reduction, only the faster mechanism operates, and when water is present during growth or reduction, both mechanisms operate simultaneously, though the contribution from the slow mechanism dominates that of the fast mechanism. Because few geologic environments are truly dry, the slower law should generally be used for modeling O diffusion for rutile in nature. Comparison with other studies of rutile suggests that migration of O vacancies is the mechanism responsible for the faster diffusion law whereas migration of Ti interstitials is responsible for the slower diffusion law.

Oxygen diffusion in rutile is slower perpendicular to the c axis than parallel to that axis by about half an order of magnitude. There is no perceptible effect of confining pressure on D below 100 MPa, or between 600 and 1000 MPa. However, between 100 and 600 MPa, D decreases by nearly an order of magnitude.

Closure temperatures for O diffusion in rutile are high—650 °C for a crystal with a 100 μm radius and a 10 °C/Ma cooling rate. Rutile is retentive of its O isotopic composition. A crystal with a 100 μm radius will retain its initial core composition for just over 10 million years at 600 °C.

Introduction

Bulk O isotope compositions of minerals in metamorphosed rock bodies can yield information regarding the temperature of mineral crystallization and the extent and nature of fluid-mineral interactions. However, the interpretation of bulk isotopic compositions is often challenging or misleading because the minerals involved might not be homogeneous—having been altered during cooling, by a secondary thermal event, or by exchange with a metasomatic fluid. Still, minerals with altered compositions can record the changes that caused the alteration and therefore have significant potential as sources of information regarding the temperature and compositional history of rock bodies.

To interpret non-uniform $^{18}O/^{16}O$ distributions in minerals, one must: (1) be able to perform accurate, in-situ micrometric analyses of O isotope ratios in natural minerals; (2) understand the theory governing isotope exchange in rock bodies; (3) know the equilibrium isotope partitioning of O in the minerals of interest; and (4) know the redistribution kinetics of O in the relevant minerals. Significant progress has been made recently on all of these fronts: (1) laser- and ion beam-ablation mass-spec-

* E-mail: DMoore@agu.org

0003–004X/98/0708–0700$05.00

trometric techniques are rapidly becoming more precise and accessible, and, for large minerals like garnet, mechanical sampling has been used (e.g., ion probe in Riciputi and Paterson 1994 and Valley et al. 1991; laser ablation in Sharp 1990, Wiechert and Hoefs 1995, and Young and Rumble 1993; mechanical sampling in Kohn et al. 1993); (2) the theory for predicting the evolution of mineral isotope compositions in rock bodies is largely developed (e.g., Giletti 1986; Eiler et al. 1992; Kohn 1993; Young 1993); (3) the database of equilibrium O isotope partitioning measurements for interesting minerals is increasing (e.g., rutile in Chacko et al. 1996); and (4) the database of O diffusion data in relevant minerals is also increasing [e.g., the reviews of Freer (1980, 1981) and Brady (1995)].

In this study, we add to the database of O diffusion in minerals by investigating O diffusion in synthetic and natural rutile under high-temperature geologic conditions. The dependence of the diffusion coefficient, D, on temperature, water pressure, crystallographic direction, and experiment duration is addressed in detail. The dependence of D on f_{O_2} and confining pressure is also addressed. The results are discussed in terms of the diffusion mechanism(s) for O in rutile, and some simple calculations are presented to convey a sense of the re-equilibration characteristics of O isotopes in rutile.

Experiments

Self-diffusion experiments of O in rutile were performed on synthetic and natural samples using an ^{18}O source. The gem-quality synthetic crystals were from a boule (grown by Atomergic Chemical Company) donated by W.G. Minarik. This material is transparent and slightly yellow. The natural rutile crystals, courtesy of A.N. Mariano (along with their PIXE-determined trace element compositions), are from the Gujar Kili emerald mine, Pakistan, and the Crab Tree emerald mine, North Carolina, U.S.A. The Gujar Kili crystals, from a talc-carbonate schist, are dark red, dense, display a roughly rectangular cross-section (2–3 mm wide and 1–2 mm long), and are elongate parallel to the c axis (4–7 mm high). The Crabtree crystals are dark red, of roughly cylindrical shape (1–3 mm in diameter), and are elongate parallel to the c axis (5–12 mm in length). Voids several hundred micrometers in diameter run the length of the Crabtree crystals. Crystal faces in natural samples display marked lineations parallel to c. Table 1 shows the trace element compositions of the samples.

Slabs no smaller than 1 mm on a side were cut parallel and perpendicular to the c axis with a low-speed diamond saw. The crystallographic orientation of synthetic samples was determined optically. Orientation of the natural samples was based on crystal form. Crystal slabs were polished with 1 μm alumina and cleaned ultrasonically. All samples were subjected to an intitial pre-anneal in air at 1400 °C for 48 h to remove crystal damage caused by cutting and polishing (e.g., Reddy and Cooper 1982).

Rutile is stoichiometric only in a nearly pure O_2 atmosphere, and crystals of different stoichiometries have different colors (e.g., Grant 1959; Frederikse 1961; Kofstad 1962). For example, crystals grown or annealed in air are honey-colored whereas those from more-reducing conditions are dark blue or black (e.g., Berkes et al. 1965). The oxidation/reduction responsible for the color change is reversible, occurs throughout the sample, and takes place quickly even at low temperatures (Cronemeyer 1952). The work of Berkes et al. (1965) on the relationship between f_{O_2} and rutile stoichiometry suggests that air-equilibrated rutile has a composition of $TiO_{1.99999}$, and that rutile equilibrated at Ni-NiO has a composition more stoichiometric than $TiO_{1.992}$.

Table 1. Rutile trace element compositions*

	Synthetic†	Gujar Kili‡	Crabtree‡
Mn	—	310	300
Fe	3730	1500	1300
V	—	9300	8600
Cr	<0.5	5100	5100
Zr	—	110	36
Nb	—	5100	1500
Ta	<0.5	63	290
W	<1	690	210
Th	<0.2	26	8
U	<0.1	4	5
Pb	—	4	3
Zn	<20	9	3
Sn	—	450	250
Cu	—	7	6
Ba	<50	0	10
La	<0.1	37	25
Ce	<1	54	70
Y	—	8	18

* Compositions reported in parts per million by weight.
† Determined by INAA.
‡ Determined by PIXE.

Seventeen of the twenty-two experiments performed were hydrothermal "cold-seal" experiments at confining pressures at or below 100 MPa (Table 2). These were prepared by placing sealed, 3 mm platinum capsules containing polished and pre-annealed rutile slabs and ~2–5 μL ^{18}O-enriched H_2O in stellite cold-seal pressure vessels, with water as the confining medium. All but two of these experiments, R23 and R27, were pre-annealed dry under atmospheric conditions and then run hydrothermally at Ni-NiO. Because rutile equilibrates quickly to new f_{O_2} conditions, the effective "pre-anneal" for these experiments occurs hydrothermally at Ni-NiO during the beginning of the experiment. To investigate whether equilibrating rutile to Ni-NiO during the beginning of the experiment affected the measured diffusion profiles, sample R27 was pre-annealed wet in water having a natural ^{18}O abundance and then run in ^{18}O-enriched water. This experiment showed that the reduction to Ni-NiO at the beginning does not effect the experimental results. To investigate the effect of water, sample R23 was pre-annealed dry at Ni-NiO, then run hydrothermally at the same f_{O_2}. The temperature of these cold-seal experiments was monitored by sheathed type-K thermocouples positioned near the sample in a well in the vessel wall and is

TABLE 2. Experimental conditions and diffusion data for oxygen in rutile

No.	T (°C)	t (s)	f_{O_2}/H_2O^p*	f_{O_2}/H_2O^r†	P_{ext}/P_{H_2O}	Type‡	D (m²/s)	$\log_{10} D$	±
Diffusion in synthetic crystals parallel to (001)									
OD27	750	1.22×10^6	atm/dry§	Ni-NiO/wet	100 MPa	n	8.9×10^{-22}	−21.05	0.11
						t	3.2×10^{-20}	−19.50	0.14
OD7	810	8.70×10^4	atm/dry§	Ni-NiO/wet	100 MPa	n	1.0×10^{-20}	−20.00	0.15
						t	1.9×10^{-19}	−18.72	0.14
OD4	850	9.84×10^4	atm/dry§	Ni-NiO/wet	100 MPa	n	1.7×10^{-20}	−19.77	0.15
						t	4.9×10^{-19}	−18.31	0.17
R9	900	8.37×10^4	atm/dry§	Ni-NiO/wet	100MPa	n	1.6×10^{-19}	−18.80	0.10
						t	9.2×10^{-19}	−18.04	0.09
R14	900	3.49×10^5	atm/dry§	Ni-NiO/wet	100 MPa	n	4.9×10^{-20}	−19.31	0.04
						t	8.9×10^{-19}	−18.05	0.11
R12	900	5.83×10^5	atm/dry§	Ni-NiO/wet	100 MPa	—	7.6×10^{-20}	−19.12	0.03
R27‖	900	1.05×10^5	Ni-NiO/wet	Ni-NiO/wet	100 MPa	n	1.3×10^{-19}	−18.89	0.03
						t	2.9×10^{-18}	−17.54	0.08
OD26	953	4.24×10^4	atm/dry§	Ni-NiO/wet	100 MPa	n	3.6×10^{-19}	−18.44	0.04
						t	4.7×10^{-18}	−17.33	0.24
OD43	1000	1.90×10^4	atm/dry§	Ni-NiO/wet	100MPa	—	1.4×10^{-18}	−17.85	0.03
OD29	900	8.64×10^4	atm/dry§	Ni-NiO/wet	600 MPa	n	1.3×10^{-20}	−19.89	0.12
OD63	900	1.73×10^5	atm/dry§	Ni-NiO/wet	10^3/<10^3MPa#	n	1.7×10^{-20}	−19.77	0.13
						t	1.7×10^{-19}	−18.77	0.13
R3	900	1.73×10^5	atm/dry§	Ni-NiO/wet	1000 MPa	n	7.4×10^{-21}	−20.13	0.20
R17	807	9.02×10^4	atm/dry	atm/dry	1 atm/none	—	1.9×10^{-19}	−18.72	0.14
R23	900	1.21×10^5	Ni-NiO/dry	Ni-NiO/wet	100 MPa	—	1.3×10^{-18}	−17.89	0.02
Diffusion in synthetic crystals perpendicular to (001)									
OD53	900	2.66×10^5	atm/dry§	Ni-NiO/wet	100 MPa	n	3.6×10^{-20}	−19.44	0.04
						t	3.5×10^{-19}	−18.46	0.11
R32	909	8.09×10^4	atm/dry§	Ni-NiO/wet	100 MPa	n	5.0×10^{-20}	−19.30	0.07
						t	3.0×10^{-19}	−18.52	0.12
R10	900	8.22×10^4	atm/dry§	Ni-NiO/wet	67 MPa	n	3.3×10^{-20}	−19.48	0.10
						t	3.8×10^{-19}	−18.42	0.14
R31	1000	1.17×10^4	atm/dry§	Ni-NiO/wet	67 MPa	n	4.5×10^{-19}	−18.35	0.09
						t	6.5×10^{-18}	−17.19	0.11
R11	900	8.04×10^4	atm/dry§	Ni-NiO/wet	33 MPa	n	3.4×10^{-20}	−19.47	0.08
						t	4.4×10^{-19}	−18.36	0.22
R33	780	2.43×10^5	atm/dry	atm/dry	1 atm/none	—	2.0×10^{-20}	−19.70	0.16
Diffusion in natural crystals parallel to (001)									
R42	909	8.09×10^4	atm/dry§	Ni-NiO/wet	100 MPa	G-n	3.9×10^{-19}	−18.41	0.06
						G-t	2.4×10^{-18}	−17.62	0.20
R50	1000	1.13×10^4	atm/dry§	Ni-NiO/wet	66 MPa	C-n	2.9×10^{-18}	−17.54	0.17
						C-t	1.6×10^{-17}	−16.80	0.05

* $f_{O_2^p}$ is the oxygen fugacity of the preanneal, H_2O^p describes if water is present during the preanneal.
† $f_{O_2^r}$ is the oxygen fugacity of the experiment, H_2O^r describes if water is present during the experiment.
‡ n is for the near-surface part of the profile, t is for the tail part; G is for Gujar Kili, C is for Crabtree.
§ Rutile equilibrates quickly to new f_{O_2} conditions; therefore, the effective "preanneal" occurs at Ni-NiO/wet during the beginning of these experiments.
‖ Preannealed wet, with water that was un-enriched in ^{18}O; run wet, with ^{18}O-enriched water.
Fluid added as a 50:50 CO_2:^{18}O-enriched H_2O mix, by weight-CO_2 added as $Ag_2C_2O_4$.

accurate to within 5 °C of that reported. Pressure was maintained to within 2% of the reported value.

Three hydrothermal "piston-cylinder" experiments were conducted at confining pressures of 600 and 1000 MPa (R3, OD29, and OD63; Table 2). Diffusion samples were made by placing slabs of polished and pre-annealed (in air) rutile along with ~2–5 μL ^{18}O-enriched H_2O in platinum-lined, surface-oxidized nickel capsules [see Watson and Cherniak (1997) for experimental details]. The effective pre-anneal for these experiments also occurs wet at Ni-NiO at the beginning of the experiment. To isolate the effects of water and confining pressure, sample OD63 was run at 1000 MPa with $P_{water} < P_{total}$. In this experiment the fluid was added as a 50:50 mix, by weight, of CO_2 (added as $Ag_2C_2O_4$) and ^{18}O-enriched H_2O. The temperature of these piston-cylinder experiments was measured by type-D thermocouples (W3%Re vs. W25%Re) and is accurate to within 10 °C of that reported.

Following hydrothermal experiments, crystals were cleaned ultrasonically in water, ethanol, and acetone. Sample surfaces maintained a good polish during hydrothermal runs, and no quench material was observed. Because the source is nearly pure $H_2{}^{18}O$ (>96% $H_2{}^{18}O$), these experiments yield very high surface concentrations of ^{18}O. Both the cold-seal and piston-cylinder apparatuses maintain the f_{O_2} of experiments near the Ni-NiO buffer. Hydrothermal experiments at the WM and MH f_{O_2} buffers were attempted but were unsuccessful because there was not enough experimental volume for the amount of solid buffer needed to maintain a fixed f_{O_2} throughout the experiment.

Two dry, 1 atm experiments, R17 and R33, also were performed (Table 2). These consisted of welded, 3 mm-

diameter platinum capsules containing polished and pre-annealed slabs of rutile surrounded by ^{18}O-enriched Al_2O_3 powder. These experiments were performed in vertical tube furnaces. The temperature was monitored just outside the sample capsules by type-K thermocouples and is accurate to within 3 °C of that reported. After the dry experiments, crystals were cleaned ultrasonically in water, ethanol, and acetone. The ^{18}O source material for these experiments was made by reacting fine-grained aluminum powder with ^{18}O-enriched water in sealed 5 mm-diameter AgPd capsules at 700 °C and 200 MPa for 24 h. Two such treatments, with intermediate grinding, were required to oxidize sufficient Al metal. The concentration of ^{18}O in the resulting solid source is 5–10 at%. This yielded surface concentrations in diffusion products of 4–6 at%, which is 20–30 times above background. Oxygen-18 enriched rutile powder was not used because it caused significant roughening of sample surfaces. Dry, low-f_{O_2} experiments were attempted, but the concentration of introduced ^{18}O in the products was lowered to unmeasurable levels by exchange with the solid O buffer.

Analysis

The distribution of ^{18}O in run products was measured by nuclear reaction analysis (NRA) using the reaction $^{18}O(p,\alpha)^{15}N$. In this method, energetic protons bombard the rutile crystal and react with ^{18}O nuclei, yielding α particles of a specific energy. The α particles lose energy in a predictable way as they pass through the rutile crystal, so the depth at which they originated can be calculated. The raw NRA spectra, which consist of plots of α particle counts vs. channel number, are converted to concentration vs. depth profiles (Cherniak 1990). All analyses were performed on the 4 MV Dynamitron linear accelerator at SUNY-Albany using a 1.65 MeV (monoenergetic) beam of H_2^+ ions (Cherniak 1990). The depth resolution of this technique is about 150 Å. One-sigma uncertainties in the concentration data, typically 2–4%, are assumed to be proportional to the square root of the number of counts from the raw NRA spectra. For more information regarding this analytical technique see Cherniak (1990), Ryerson et al. (1989), or Amsel and Lanford (1984).

Simple profiles

Experiments were designed so that resulting concentration profiles could be modeled by the analytical "constant surface concentration" solution to the diffusion equation (Shewmon 1989):

$$C(x,t) = C_0\left[1 - \mathrm{erf}\left(\frac{x}{\sqrt{4Dt}}\right)\right] \quad (1)$$

where C is the concentration at depth x and time t, C_0 is the surface concentration, and D is the diffusion coefficient. This solution is valid for one-dimensional diffusion via a single mechanism into a semi-infinite space from a surface with constant, uniform concentration. All our experiments satisfy these constraints. Tannhauser (1956) explains why the powder source configuration is satisfactory.

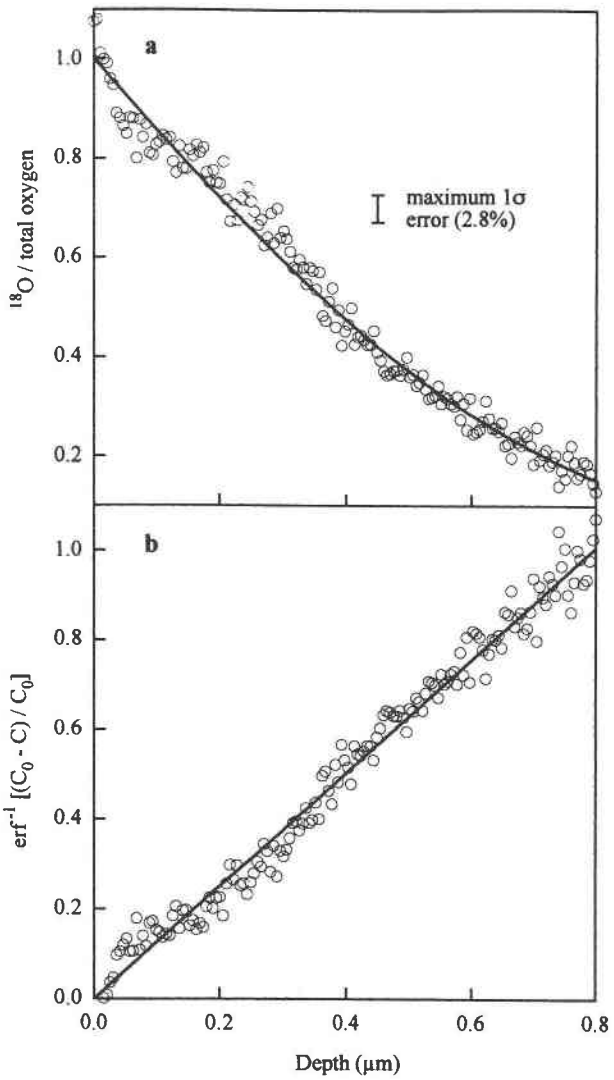

Figure 1. (**a**) Diffusion profile of sample R23, which was dry-reduced to Ni-NiO then run hydrothermally at Ni-NiO. Symbols represent data, with associated errors as shown; line is a complementary error function curve (Eq. 1); the surface concentration, C_0, and D are determined from the fit in b. (**b**) Linearization of the data in a by inversion through the error function. Symbols are data; line is the fit from regression and has slope $1/(4Dt)^{1/2}$.

The three experiments using rutile that had not been reduced in the presence of water were modeled using Equation 1 (two dry experiments: R17 and R33; one hydrothermal: R23. Fig. 1a). Data from these experiments form a straight line, with slope $1/(4Dt)^{1/2}$, on plots of the inverse of the error function of $\{[C_0\text{-}C(x,t)]/C_0\}$ vs. depth, x (Fig. 1b). Diffusivities were extracted from the slopes of the lines fit to the data by least-squares regression (Fig. 1b). Because the solution is constrained to pass through

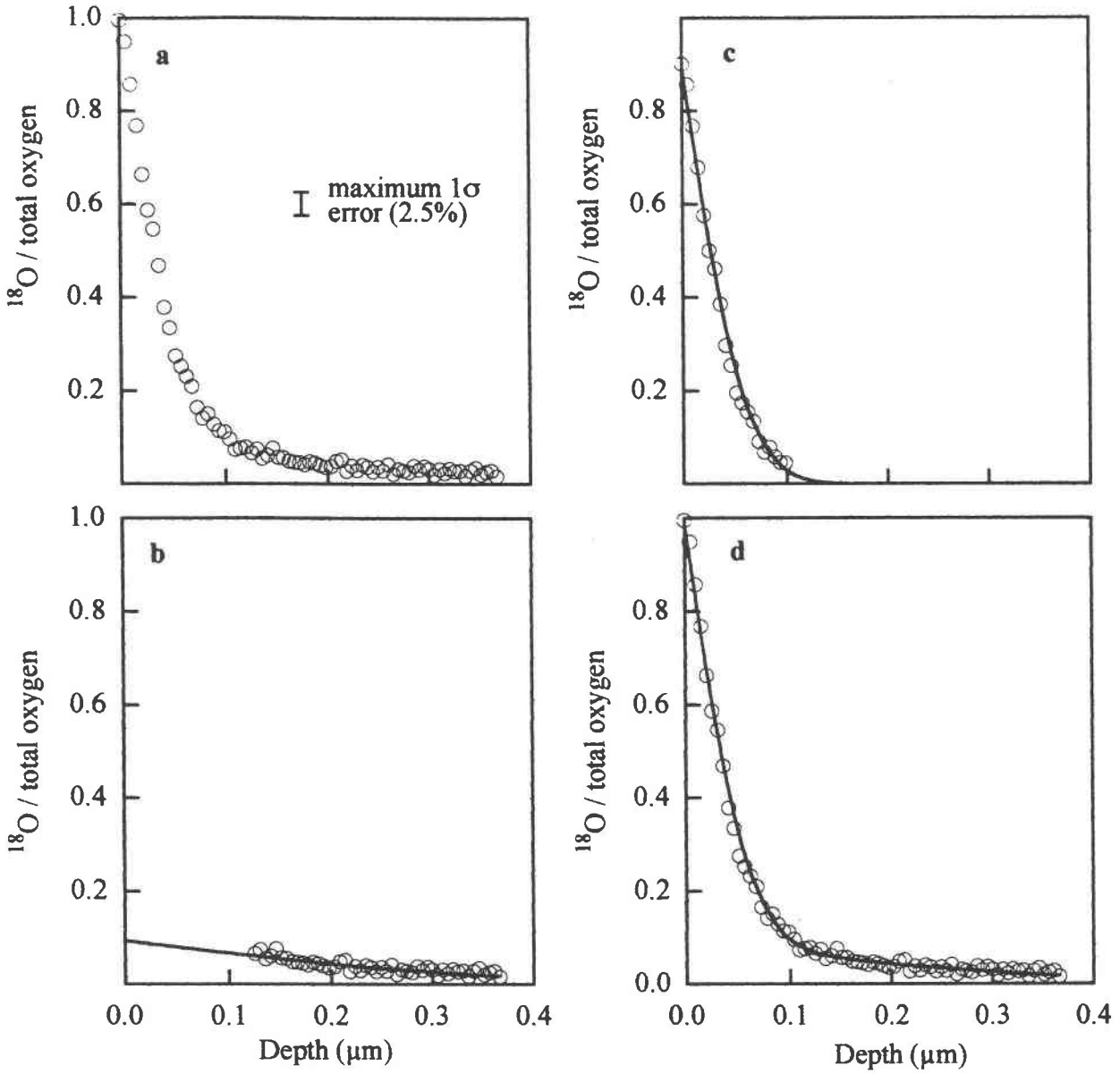

FIGURE 2. (**a**) Diffusion profile of sample OD27, a profile typical of wet-reduced samples. Notice the "tailing." Maximum error in data as indicated. (**b**) Error function fit to the tail portion of the profile. Symbols are data, line is the fit (using Eq. 1). (**c**) Error function fit to the residual profile. Symbols are residual-concentration data points calculated by subtracting the error function fit in b from the data in a; line is the fit (using Eq. 1). (**d**) Fit of data in a by the linear combination of the error functions shown in b and c.

zero, this method produces an independent determination of C_0, which cannot be measured directly.

Composite profiles

The 19 experiments using rutile that had been reduced in the presence of water yielded profiles with more ^{18}O at depth than would be introduced by a single volume diffusion mechanism (Fig. 2a). This feature is often referred to as "tailing" and is commonly indicative of a rapid diffusion mechanism or pathway. We attempted to fit these profiles with a single error function, but this method failed to account for the tail region. To determine if these profiles could be considered as the combination of two error functions, we carried out an analysis of variance using the F-test statistic. This is a statistical analysis in which the variance of a "one-function" fit was compared with that of a "two-function" fit. The value of F determined for the wet-reduced profiles indicated a two-function fit at the >99% confidence level. The two-function fit used in the statistical analysis was the following:

$$C(x,t) = a_1 C_{0,1}\left[1 - \mathrm{erf}\left(\frac{x}{\sqrt{4D_1 t}}\right)\right] + a_2 C_{0,2}\left[1 - \mathrm{erf}\left(\frac{x}{\sqrt{4D_2 t}}\right)\right] \quad (2)$$

where a_1 and a_2 are the coefficients of each error function term and represent the interdependence of the two functions, and the other variables are as for Equation 1. In all cases, both a_1 and a_2 were, within error, equal to 1, suggesting that the two error functions are statistically independent. This does not mean that the mechanisms responsible for the functions are physically independent, only that the interaction between the mechanisms is small enough to not be measurable. Furthermore, because the tails are fairly flat, it is not possible to demonstrate that they are indeed error functions. However, Boltzmann-Matano analysis, which allows D to be calculated at each point along a particular profile (Shewmon 1989), shows that as long as a function is chosen that fits the tail data well, the D that is extracted from the tail is the same. Our time-series experiments suggest that both the near-surface and tail regions of the profile are the result of lattice diffusion. We interpret these profiles as representing O diffusion via two simultaneously acting, statistically independent mechanisms.

Diffusivities were extracted from these wet-reduced profiles using a less general version of the Equation 2 approach (Fig. 2b–d). First, that portion of the tail region which is devoid of contribution from the near-surface mechanism was fit by an error function using Equation 1 (Fig. 2b). Then this error function fit was subtracted from the original C-x profile, resulting in a profile that is fit by a second error function (Fig. 2c). The fit to the entire profile was then generated by summing these two error function fits (Fig. 2d). Having realized that this method of fitting the data assumed the statistical independence of the two mechanisms, the validity of the assumption was investigated as described previously, using the fully general fitting procedure of Equation 2 and performing the F-test. The profiles were not refit using the fully general approach because the assumption of the first method proved to be valid and because both methods produced the same diffusivities.

Results

Most experiments investigated the dependence of D on temperature, water pressure, crystallographic direction, and experiment duration. A few experiments investigated the dependence of D on f_{O_2} and confining pressure. Table 2 contains the pre-anneal and experimental conditions and results. Figure 3 shows results for diffusion parallel to c. Figure 4 shows the variation of D with water and confining pressure (Fig. 4a), crystallographic direction (Fig. 4b), and experiment duration (Fig. 4c).

Most experiments were hydrothermal at Ni-NiO using rutile that had been pre-annealed dry at 1 atm and then wet-reduced to Ni-NiO during the beginning of the experiment. The experiment with sample R27, which was pre-annealed at Ni-NiO in undoped water before running it hydrothermally at Ni-NiO, showed that reducing rutile to Ni-NiO at the beginning of the experiment gives the same results as reducing it in a pre-anneal. These experiments yield the two-error-function composite profiles described previously (Fig. 2). Two D values are extracted from each of these experiments, one from the near-surface region of the profile and one from the tail region (Table 2; Figs. 2 and 3). The diffusivities from the near-surface region of these profiles are described by the slower diffusion law of Figure 3, which has a pre-exponential factor of 5.9×10^{-5} m²/s and an activation energy of 330 ± 15 kJ/mol.

Two of the experiments, R17 and R33, used dry 1 atm rutile that had been pre-annealed dry at 1 atm. One experiment, R23, was pre-annealed dry at Ni-NiO and run wet at Ni-NiO. These three experiments used rutile that either had not been reduced or had been reduced in the absence of water. Diffusivities from these three experiments, together with the diffusivities from the tail region of the composite profiles, are described by the faster diffusion law of Figure 3, which has a pre-exponential factor of 4.7×10^{-7} m²/s and an activation energy of 258 ± 22 kJ/mol.

Effect of water and f_{O_2} on D

The differences in diffusion behavior between those experiments in which O diffuses by both mechanims and those in which O diffuses by only the faster mechanism seem to result from the presence of water during reduction of rutile. Sample R23, which was dry-reduced and then run hydrothermally, supports this conclusion. Despite being run hydrothermally, it produced profiles like those from the two 1 atm experiments. So, O diffusion in wet-reduced rutile proceeds by two mechanisms, according to both the measured diffusion relations, and in non- or dry-reduced rutile by one mechanims only, according to the faster diffusion relation. With respect to the amount of O moved in wet-reduced rutile, the slower mechanism dominates. In fact, for "long" anneals, the contribution from the faster mechanism can be ignored (see discussion of the variation of D with time). The effect of water on O diffusion in rutile is altogether different from its effect on silicates and other oxide minerals like magnetite, for which O diffusion is faster in the presence of water (e.g., quartz in Gilleti and Yund 1984; feldspars in Giletti et al. 1978; diopside in Farver 1989; zircon in Watson and Cherniak 1997; magnetite in Giletti and Hess 1988). Consequently, though speciation (i.e., O moving as O^{2-}, OH^-, or H_2O) explains the effect of water on O diffusion in some silicates (e.g., Doremus 1969; Zhang et al. 1991), it clearly does not explain the effect in rutile.

The mechanism responsible for the faster diffusion relation is independent of f_{O_2} from 1 atm to Ni-NiO. Experiments run at Ni-NiO (R23) and at 1 atm (R17 and R33) yield diffusivities that are described by the same diffusion relation (Fig. 3). It was not possible to test whether the mechanism responsible for the O diffusion behavior in wet-reduced rutile is independent of f_{O_2} over geologic conditions because, as mentioned, the attempted experiments at f_{O_2} of the WM and MH buffers were unsuccessful.

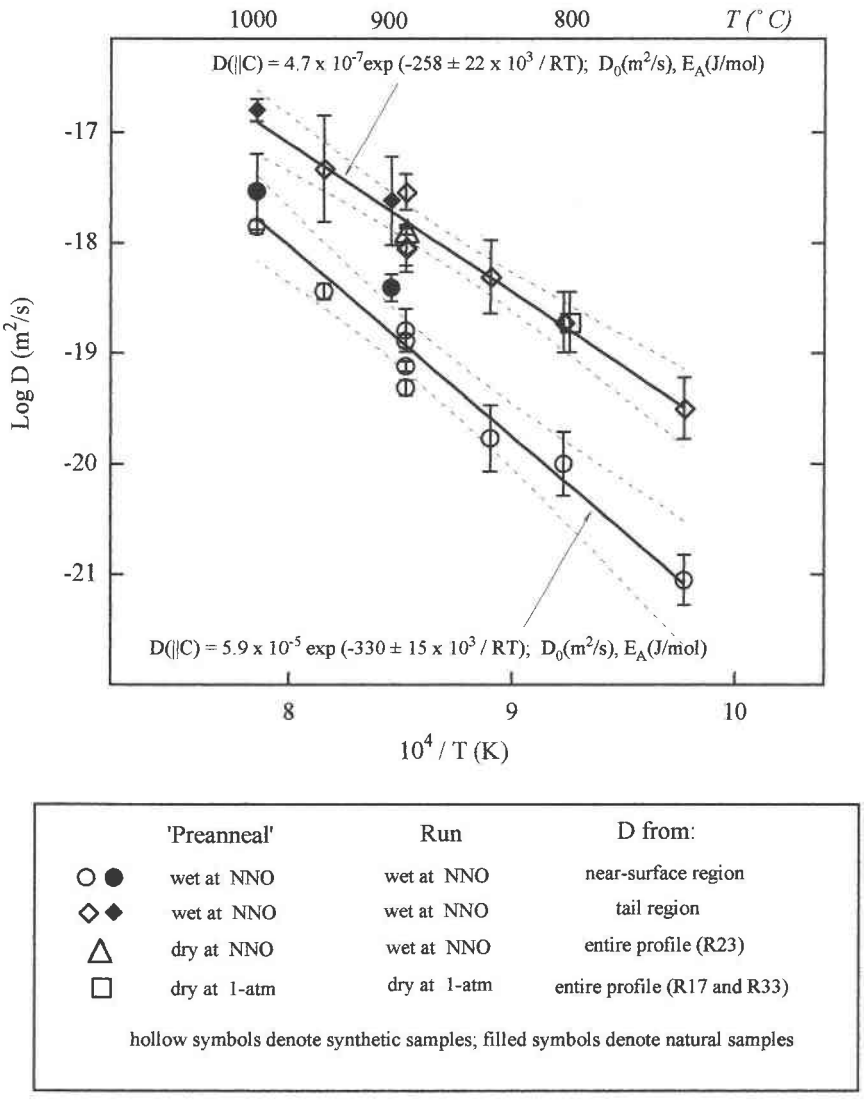

FIGURE 3. Oxygen diffusion in rutile parallel to the *c* axis. Symbols are data points; error bars represent 2σ errors. Solid lines are least-squares fits to data; dashed lines represent the 99% confidence intervals for the fits. Equations give the diffusion law for each line.

Effect of pressure on *D*

The dependence of *D* on water and total pressure was investigated by examining diffusion perpendicular to (≤100 MPa, Fig. 4a) and parallel to the *c* axis (100–1000 MPa, Fig. 4a). *D* was not observed to vary over the pressure ranges 1 atm to 100 MPa and 600–1000 MPa (Fig. 4a), but the *D* values of the high-pressure experiments are about an order of magnitude slower than for the low-pressure experiments (Fig. 4a). Experiment OD63, which had $P_{H_2O} < P_{total}$ = 1000 MPa, yielded a diffusivity within error of those from the $P_{H_2O} = P_{Total}$ = 600 and 1000 MPa experiments, suggesting that confining pressure is probably responsible for the decrease in *D* between 100 and 600 MPa.

Variation of *D* with crystallographic direction

Diffusion of O in rutile is about half an order of magnitude slower perpendicular to the *c* axis than parallel to it (Fig. 4b). This is consistent with observations that the thermal conductivity of rutile is fastest parallel to the *c* axis (McCarthy et al. 1952). Structurally, rutile has a slightly more open structure parallel to the *c* axis, which could be the reason why $D_0(\|c)$ is larger than $D_0(\perp c)$. Because the range of temperature of our $D(\perp c)$ experiments was only 200 °C, we fit the data in Figure 4b by varying the pre-exponential factors of the $D(\|c)$ diffusion laws. This method assumes that the activation energy is not a function of crystallographic direction, which seems reasonable because Ti-O bond lengths and strengths in rutile are largely independent of crystallographic direction (Grant 1959).

Variation of *D* with experiment duration

The variation of *D* with experiment duration was investigated to demonstrate that the measured diffusion profiles were the result of lattice diffusion only. There is no dependence of *D* on experiment duration (Fig. 4c), and zero-time experiments yielded profiles identical to pro-

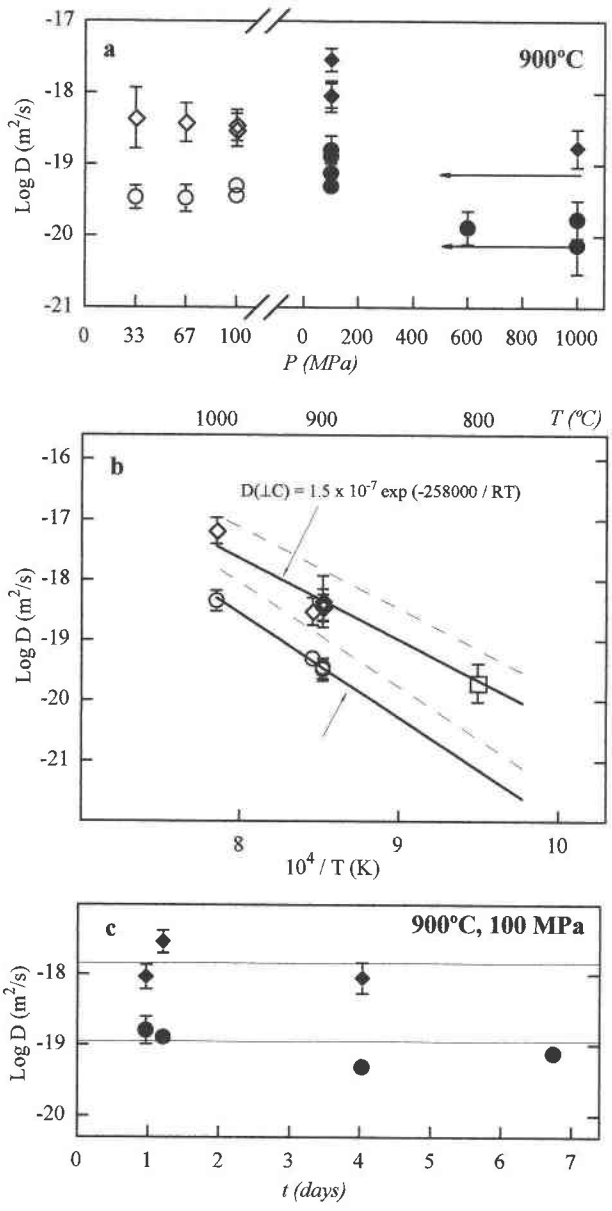

FIGURE 4. Symbols are as for Figure 3, except in this figure hollow symbols denote diffusion $\perp c$ and filled symbols denote diffusion parallel to c. (**a**) Pressure dependence of diffusivity for experiments conducted at 900 °C. Water pressure equals confining pressure for all samples except for OD63, for which arrows indicate that $P_{H_2O} < P_{Total}$. (**b**) Oxygen diffusion in rutile perpendicular to the c axis. Dashed lines are the diffusion laws from Figure 3. The solid lines were created by varying the D_0 value—and holding the E_A value constant—so as to fit the data (see text for details). Equations are the diffusion laws that fit the data. (**c**) Time dependence of $D(\|c)$ for experiments conducted at 900 °C and 100 MPa. Lines are the diffusivities calculated from the diffusion laws of Figure 3.

files from experiment "blanks." Therefore, the measured diffusivities likely represent "lattice" diffusion, with no contribution from chemical alteration, transient diffusion paths, etc. No tail-diffusivity is reported for the long-duration experiments, e.g., R12 and OD43, because the contribution to the profile from the near-surface diffusion mechanism overwhelms the contribution from the tail mechanism for these times. As a result, contributions from the two mechanisms can be distinguished only when experimental times are sufficiently short to keep the contribution from the near-surface mechanism very near the surface.

DISCUSSION

The mechanisms responsible for diffusion of both O and Ti in rutile are controlled largely by defect chemistry (Haul and Dümbgen 1965; Venkatu and Poteat 1969; Grant 1959). In this section, we summarize the results of studies bearing on the mechanisms responsible for diffusion in rutile and draw some conclusions about the mechanisms.

Table 3 summarizes the results of diffusion studies of rutile. All the studies cited therein used synthetic rutile and studied diffusion parallel to the c axis. Their results are essentially identical to the faster of the two diffusion laws observed by us (Table 3). The Haul and Dümbgen (1965) and Derry et al. (1981) O diffusion data are from gas-exchange experiments. Both studies concluded that O diffusion is extrinsic and is the result of the migration of O vacancies. The Venkatu and Poteat (1969) and Akse and Whitehurst (1978) Ti diffusion data are from thin source, surface tracer deposit experiments. Both studies concluded that under dry conditions Ti diffusion in rutile is extrinsic and is the result of O vacancy migration. In addition to dry experiments, Akse and Whitehurst (1978) performed experiments on rutile that was reduced using an H_2/H_2O buffer. Under these conditions, they observed a higher activation energy. They concluded that Ti diffusion in rutile under wet, reducing conditions results from the migration of Ti interstitials. Their results, showing that Ti diffusion behavior is different for rutile that has been reduced in the presence of water, are consistent with our observations of O diffusion behavior.

Chester (1961) studied the electron spin resonance of nonstoichiometric rutile and observed that samples reduced by H produced unique spectra. He interpreted these spectra as the result of either Ti^{3+} interstitials or Ti^{3+} interstitials associated with O vacancies. The presence of Ti^{3+} interstitials under these conditions is supported by the observations of Young et al. (1961) concerning the weak hyperfine structure of rutile. However, O vacancies clearly are also present. Gray (1957) reported that reduction of rutile in a H atmosphere involves a weight loss. Moreover, the tails of wet-reduced experiments and the profiles of non- and dry-reduced experiments are described by the same diffusion law (Fig. 2). Kofstad (1967) synthesized the available data and concluded that the defect structure of rutile is dominated by O vacancies at

TABLE 3. Summary of diffusion studies of rutile

El	T (°C)	H_2O	P_{O_2} (atm)	Mechanism	D_0 (m^2/s)	E_A (kJ/mol)	Ref.*
O	750–1000	dry†	atm/Ni-NiO	O vacancies	4.7×10^{-7}	258 ± 22	current
O	750–1000	wet‡	Ni-NiO	Ti interstitials§	5.9×10^{-5}	330 ± 15	current
O	710–1300	dry	10^{-3}–10^{3}	O vacancies	2×10^{-7}	251 ± 6	H&D
O	900–1200	dry	1	O vacancies	2.4×10^{-6}	283 ± 5	D
Ti	900–1300	dry	1	O vacancies	6.4×10^{-6}	257	V&P
Ti	1000–1100	dry	1	O vacancies	6.4×10^{-6}	257	A&W
Ti	1000–1100	wet	10^{-14}–10^{-17}	Ti interstitials	$3.3 \times 10^{+6}$	465	A&W

* References are: current = this study; H&D = Haul and Dümbgen (1965); D = Derry et al. (1981); V&P = Venkatu and Poteat (1969); A&W = Akse and Whitehurst (1978).
† By dry is meant that the rutile used was not reduced or was reduced in the absence of water.
‡ By wet is meant that the rutile used was reduced in the presence of water.
§ Migration of Ti interstitials dominates, but O vacancies are also present.

low temperatures and high O pressures and by Ti interstitials at high temperatures and low O pressures. Chester (1961), Young et al. (1961), and Gray (1957) all observed a change in the behavior (defect structure) of rutile in samples that had been reduced in the presence of H, suggesting that it is the H in the water, and not the water itself, that is responsible for the effects of "water" on diffusion that we observe.

We suggest the following as a likely model for diffusion mechanisms in rutile: (1) for non- and dry-reduced rutile, diffusion occurs via migration of O vacancies; and (2) for wet-reduced rutile, diffusion occurs dominantly via the migration of Ti^{3+} interstitials, with a subordinate contribution from migration of O vacancies. The reactions for reduction under the two conditions are possibly the following:
dry reduction:

$$Ti_L^{4+} + 2O_L^{2-} \rightarrow Ti_L^{4+} + O\square + O_L^{2-} + 2e^- + \tfrac{1}{2}0_2(g)$$

reduction in the presence of H:

$$Ti_L^{4+} + 2O_L^{2-} + H^+ + 3e^- \rightarrow Ti_I^{3+} + OH_L^- + O_L^{2-}$$

or

$$Ti_L^{4+} + 2O_L^{2-} + \tfrac{1}{2}H_2 + 2e^- \rightarrow Ti_I^{3+} + OH_L^+ + O_L^{2-}$$

where the subscripts L, $\square$, and I denote a filled lattice site, a vacant lattice site, and an interstitial atom, respectively. Though this model accounts for the observations of the diffusion behavior in rutile made to date, it should be emphasized that it only can be considered a likely possibility.

Fortier and Giletti (1989) developed a predictive model for O diffusion in silicates based on calculations of the ionic porosity of minerals (see also Dowty 1980). Their model does not predict D values accurately for rutile. In fact, the predicted D values are never closer than six orders of magnitude. There is, however, no reason to expect the model to compare favorably with the experimental data for rutile because the model is designed for silicates. An additional possible explanation is that O diffusion in rutile is extrinsic, whereas ionic porosity is a measure of an intrinsic property of a crystal.

APPLICATIONS

We expect the primary geologic use of these data to be extraction of T-t or X-t information from the non-homogeneous O isotope compositions of minerals in metamorphic or igneous rock bodies. After discussing the geologic occurrence of rutile and which diffusion relation should be used for modeling a given set of geologic conditions, we present the results of some simple calculations aimed at giving the reader a feel for the diffusion dependent re-equilibration characteristics of O isotopes in rutile.

Rocks that form at high pressure or contain abundant Ti and low Fe/Mg commonly include rutile as an accessory phase. These include granitic rocks, eclogites, amphibolites, schists, gneisses, upper-mantle rocks, and meta-limestones. In these rocks, rutile commonly occurs as acicular inclusions in other minerals (e.g., mica, pyroxene, olivine, quartz, corundum, and garnet).

Inasmuch as rutile is stoichiometric only in a nearly pure O_2 atmosphere, all natural rutile is non-stoichiometric or "reduced." Because the O diffusion behavior of rutile depends on the environment in which it grew or was reduced, choosing a diffusion law for modeling requires understanding the nature of that environment. If rutile grew or was reduced in the presence of water, then the wet-reduced diffusion relation should be used for modeling. For those rare environments that are truly anhydrous, the non- or dry-reduced diffusion relation should be used. Because rutile crystals in nature resemble elongated cylinders, diffusive re-equilibration will be dominated typically by diffusion perpendicular to the c axis. Therefore, a diffusion relation for $D(\perp c)$ should be used to model this process. Moreover, to avoid the effects of re-equilibration parallel to the c axis, compositional profiles of natural samples should be measured as far from the ends of the crystal as possible. We suggest that, for pressures below several hundred megapascals, no confining-pressure effect need be taken into account and that, for pressures exceeding about 400 MPa, the diffusion relation should be modified for the effect of confining pressure (i.e., up to at least 1000 MPa, it should be lowered by about an order of magnitude; see Fig. 4a). In the mod-

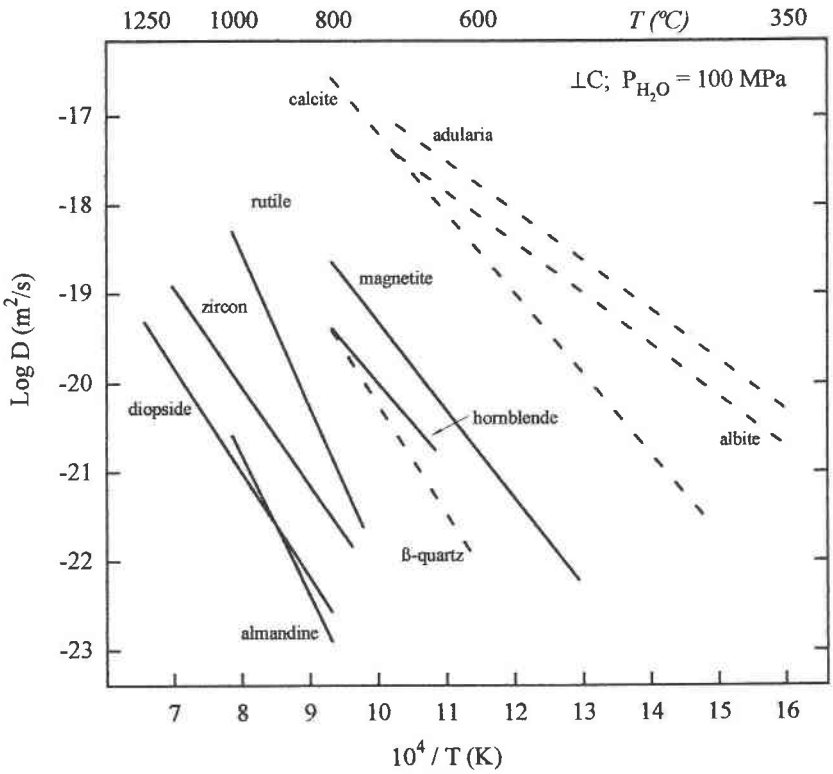

FIGURE 5. O-diffusion in rutile and in those minerals likely to coexist with rutile (diffusion ⊥ c; P_{H_2O} = 100 MPa). Dashed lines are for those minerals that more strongly partition ^{18}O; solid lines are for those that more strongly partition ^{16}O. Data for rutile from this study; almandine from Coghlan (1990); diopside from Farver (1989); β-quartz from Giletti and Yund (1984); hornblende from Farver and Giletti (1989); calcite from Farver (1994); and albite and adularia from Giletti et al. (1978).

eling presented below, we use the wet-reduced diffusion law for $D(\perp c)$, unmodified for the effects of confining pressure.

Figure 5 is a summary of O diffusion data for minerals with which rutile is likely to coexist. One of the salient features of this plot is that many of the activation energies are roughly equal. This is not surprising because, with respect to O, many of these minerals have similar structures. Oxygen isotope geothermometers are based on mineral pairs whose relative O isotope compositions are fairly strong functions of temperature. In Figure 5, minerals that more strongly partition ^{18}O are represented by dashed lines, while others are represented by solid lines. Relative to many of the other minerals, O diffuses fairly slowly in rutile. Consequently, we expect that it will have relatively high closure temperatures and be fairly retentive of its O isotope compositions.

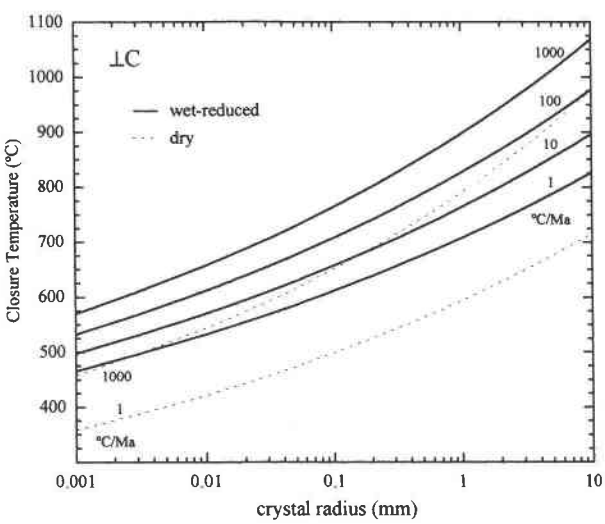

FIGURE 6. Plot of the closure temperature for O isotope exchange in rutile vs. crystal size using our $D(\perp c)$ data (100 MPa) and cooling rates as noted.

Oxygen isotope re-equilibration in rock bodies is a function of their thermal and compositional history, the relative diffusivities of O in constituent minerals, grain form, and mineral mode (Eiler et al. 1992). The method of Dodson (1973) for calculating closure temperatures does not take all of these factors into account, but it does allow the re-equilibration characteristics of minerals to be readily assessed. To demonstrate the O isotope re-equilibration behavior of rutile, we performed simple closure temperature calculations using the expression of Dodson (1973):

$$T_c = \frac{E_A/R}{\ln\left(\frac{ART_c^2(D_0/a^2)}{E_A(dT/dt)}\right)}$$

where E_A is the activation energy, R is the gas constant, A is a geometrical factor (27 for a cylinder), D_0 is the pre-exponential factor, a is the effective diffusion radius, and dT/dt is the cooling rate of the rock body. Figure 6

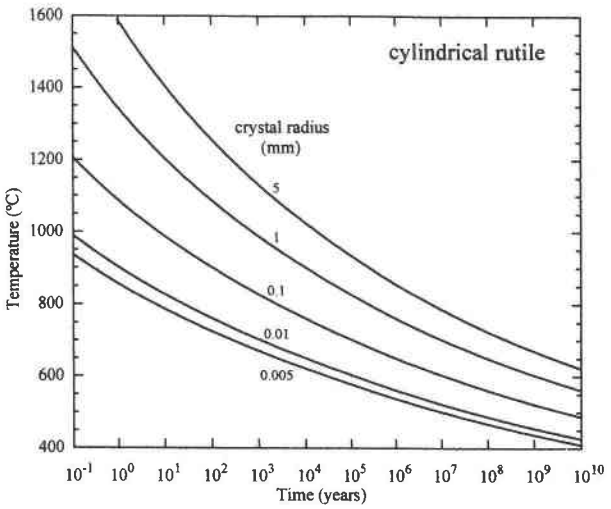

FIGURE 7. Temperature-time conditions for preservation of initial $^{18}O/^{16}O$ composition in the core of a cylindrical rutile crystal with a particular radius, a. The lines plotted are for Dt/a^2 = 0.04. For conditions below a line, the initial O isotope composition at the center of the crystal is preserved.

shows the results of these calculations for rutile. A rutile crystal with an effective diffusion radius of 0.05 mm would have a closure temperature of 629 °C (Fig 6). In spite of its typically small crystal size, rutile exhibits a relatively high closure temperature. Rutile has a much higher closure temperature than magnetite (for magnetite, see Giletti and Hess 1988). Rutile and quartz, which commonly occur together in the same rocks, form a very useful mineral pair because they both have high relative closure temperatures (for quartz, see Giletti and Yund 1984). Rutile will be a good thermometer under various geologic conditions because it has a high closure temperature, is often found in low abundace in a rock, and strongly partitions ^{16}O (Chacko et al. 1996).

To assess how retentive rutile is of its initial $^{18}O/^{16}O$ composition during a thermal event, we performed calculations using an analytical solution to the diffusion equation for a cylindrical rutile grain with radius a and initial (uniform) composition C_i, which is out of equilibrium with the composition of the surrounding material, C_{ext} (Crank 1975). At the center of the cylinder (r = 0) the following relation holds:

$$\frac{C - C_i}{C_{ext} - C_i} 1 - 2 \sum_{n=1}^{\infty} \frac{\exp[-\beta_n^2 (Dt/a^2)]}{\beta_n J_1(\beta_n)} \qquad (4)$$

where the β_n terms are the positive roots of the zeroth-order Bessel function of the first kind, i.e., $J_0(\beta_n) = 0$. For a cylinder, when the dimensionless parameter Dt/a^2 is less than 0.04, the concentration at the center of the crystal remains unperturbed by the effects of the external concentration (Crank 1975). Thus, this relation allows one to determine the T-t conditions that result in preservation of the initial isotopic composition at the center of a rutile crystal. Figure 7 shows the results of these calculations. For conditions below the curves, the center of a rutile crystal retains its initial composition. A rutile crystal with r = 0.1 mm loses its initial composition only after heating at 600 °C for just over 10 million years. It should be emphasized that these calculations represent the upper limit for geologic re-equilibration because geologic heating events are not isothermal. Based on these calculations, we conclude that despite its typically small grain-size, rutile retains its initial O-isotope composition during a wide range of thermal events.

ACKNOWLEDGMENTS

We thank W.G. Minarik for donation of the synthetic rutile and A.N. Mariano for donation of the natural rutile. An early version of this paper benefitted from the review of Minoru Tomozawa. The work was supported by the Division of Earth Sciences of the National Science Foundation, under grant EAR-9527014 awarded to E.B. Watson.

REFERENCES CITED

Akse, J.R. and Whitehurst, H.B. (1978) Diffusion of titanium in slightly reduced rutile. Journal of the Physics and Chemistry of Solids, 39, 457–465.

Amsel, G. and Lanford, W.A. (1984) Nuclear reaction techniques in materials analysis. Annual Reviews in Nuclear Particle Science, 34, 435–460.

Berkes, J.S., White, W.B., and Roy, R. (1965) Growth of rutile of controlled composition from borate fluxes. Journal of Applied Physics, 36, 3276–3280.

Brady, J.B. (1995) Diffusion data for silicate minerals, glasses, and liquids. In T.J. Ahrens, Ed., Mineral physics and cystallography: a handbook of physical constants, American Geophysical Union Reference Shelf 2, p. 269–290. American Geophysical Union, Washington, D.C.

Chacko, T., Hu, X., Mayeda, T.M., Clayton, R.N., and Goldsmith, J.R. (1996) Oxygen isotope fractionations in muscovite, phlogopite and rutile. Geochimica et Cosmochimica Acta, 60, 2595–2608.

Cherniak, D.J. (1990) A particle accelerator based study of major and trace element diffusion in minerals. Ph.D. thesis, State University of New York at Albany, Albany, 184 p.

Chester, P.F. (1961) Electron spin resonance in semiconducting rutile. Journal of Applied Physics, 32, 2233–2236.

Coghlan, R.A.N. (1990) Studies in diffusional transport: grain boundary transport of oxygen in feldspars, strontium and the REE's in gairnet, and the thermal histories of granitic intrusions in south-central Maine using oxygen isotopes, 237 p. Ph.D. thesis, Brown University, Providence.

Crank, J. (1975) The mathematics of diffusion. 2nd edition, 414 p. Oxford University Press, New York.

Cronemeyer, D.C. (1952) Electrical and optical properties of rutile single crystals. The Physical Review, 87, 876–891.

Derry, D.J., Lees, D.G., and Calvert, J.M. (1981) A study of oxygen self-diffusion in the c-direction of rutile using a nuclear technique. Journal of the Physics and Chemistry of Solids, 42, 57–64.

Dodson, M.H. (1973) Closure temperature in cooling geochronological and petrological systems. Contributions to Mineralogy and Petrology, 40, 259–274.

Doremus, R.H. (1969) The diffusion of water in fused silica. In J.W. Mitchell, R.C. DeVries, R.W. Roberts, and P. Cannon, Eds., Reactivity of solids, p. 667–673. Wiley, New York.

Dowty, E. (1980) Crystal-chemical factors affecting the mobility of ions in minerals. American Mineralogist, 65, 174–182.

Eiler, J.M., Baumgartner, L.P., and Valley, J.M. (1992) Intercrystalline stable isotope diffusion: a fast grain boundary model. Contributions to Mineralogy and Petrology, 112, 543–557.

Farver, J.R. (1989) Oxygen self-diffusion in diopside with application to cooling rate determinations. Earth and Planetary Science Letters, 92, 386–396.

——(1994) Oxygen self-diffusion in calcite: dependence on tempera-

ture and water fugacity. Earth and Planetary Science Letters, 121, 575–587.

Farver, J.R. and Giletti, B.J. (1989) Oxygen diffusion in amphiboles. Geochimica et Cosmochimica Acta, 49, 1403–1411.

Fortier, S.M. and Giletti, B.J. (1989) An empirical model for predicting diffusion coefficients in silicate minerals. Science, 245, 1481–1484.

Frederikse, H.P.R. (1961) Recent studies on rutile (TiO_2). Journal of Applied Physics, 32, 2211–2215.

Freer, R. (1980) Bibliography, self-diffusion and impurity diffusion in oxides. Journal of Materials Science, 15, 803–824.

——— (1981) Diffusion in silicate minerals and glasses: a data digest and guide to the literature. Contributions to Mineralogy and Petrology, 76, 440–454.

Giletti, B.J. (1986) Diffusion effects on oxygen isotope temperatures of slowly cooled igneous and metamorphic rocks. Earth and Planetary Science Letters, 77, 218–228.

Giletti, B.J. and Yund, R.A. (1984) Oxygen diffusion in quartz. Journal of Geophysical Research, 89, 4039–4046.

Giletti, B.J. and Hess, K.C. (1988) Oxygen diffusion in magnetite. Earth and Planetary Science Letters, 89, 115–122.

Giletti, B.J., Semet, M.P., and Yund, R.A. (1978) Studies in diffusion: III. Oxygen in feldspars: an ion microprobe determination. Geochimica et Cosmochimica Acta, 42, 45–57.

Grant, F.A. (1959) Properties of rutile (titanium dioxide). Reviews of Modern Physics, 31, 646–674.

Gray, T.J. (1957) The defect solid state, 427 p. Interscience Publishers, New York.

Haul, R. and Dümbgen, G. (1965) Oxygen self-diffusion in rutile crystals (in German). Journal of the Physics and Chemistry of Solids, 26, 1–10.

Kofstad, P. (1962) Thermogravimetric studies of the defect structure of rutile (TiO_2). Journal of the Physics and Chemistry of Solids, 23, 1579–1586.

——— (1967) Note on the defect structure of rutile (TiO_2). Journal of the Less-Common Metals, 13, 635–638.

Kohn, M.J. (1993) Modeling of prograde mineral $\delta^{18}O$ changes in metamorphic systems. Contributions to Mineralogy and Petrology, 113, 249–261.

Kohn, M.J., Valley, J.W., Elsenheimer, D., and Spicuzza, M.J. (1993) O Isotope zoning in garnet and staurolite: Evidence for closed-system mineral growth during regional metamorphism. American Mineralogist, 78, 988–1001.

McCarthy, K.A., Ballard, S.S., and Doerner, E.C. (1952) Thermal conductivity of sapphire and rutile as a function of temperature. Physical Review, 88, 153.

Reddy, K.P.R. and Cooper, A.R. (1982) Oxygen diffusion in sapphire. Journal of the American Ceramic Society, 65, 634–638.

Riciputi, L.R. and Paterson, B.A. (1994) In-situ analysis of oxygen isotope ratios in silicates and carbonates by ion microprobe. Mineralogical Magazine, 58, 770–771.

Ryerson, F.J., Durham, W.B., Cherniak, D.J., and Lanford, W.A. (1989) Oxygen diffusion in olivine: effect of oxygen fugacity and implications for creep. Journal of Geophysical Research, 94, 4105–4118.

Sharp, Z.D. (1990) A laser-based microanalytical method for the in situ determination of oxygen isotope ratios of silicates and oxides. Geochimica et Cosmochimica Acta, 54, 1353–1357.

Shewmon, P. (1989) Diffusion in Solids, 246 p. The Minerals, Metals & Materials Society, Warrendale, Pennsylvania.

Tannhauser, D.S. (1956) Concerning a systematic error in measuring diffusion constants. Journal of Applied Physics, 27, 662.

Valley, J.W., Elsenheimer, D., and Graham, C.M. (1991) Microanalysis of oxygen isotope ratios. Geologic Society of America Abstracts with Programs, 23, 101.

Venkatu, D.A. and Poteat, L.E. (1969) Diffusion of titanium in single crystal rutile. Journal of Materials Science and Engineering, 5, 258–262.

Watson, E.B. and Cherniak, D.J. (1997) Oxygen diffusion in zircon. Earth and Planetary Science Letters, 148, 527–544.

Weichert, U. and Hoefs, J. (1995) An excimer laser-based micro analytical preparation technique for in-situ oxygen isotope analysis of silicate and oxide minerals. Geochimica et Cosmochimica Acta, 59, 4093–4101.

Young, C.G., Shuskus, A.J., and Gilliam, O.R. (1961) Electron spin resonance of irradiated rutile. Bulletin of the American Physical Society, 6, 248.

Young, E.D. (1993) On the $^{18}O/^{16}O$ record of reaction progress in open and closed metamorphic systems. Earth and Planetary Science Letters, 117, 147–167.

Young, E.D. and Rumble, D. III (1993) Determination of metamorphic relation histories using small-scale maps of mineral $^{18}O/^{16}O$. Terra Abstracts, 5, 379.

Zhang, Y., Stolper, E.M., and Wasserburg, G.J. (1991) Diffusion of a multi-species componenet and its role in oxygen and water transport in silicates. Earth and Planetary Science Letters, 103, 228–240.

MANUSCRIPT RECEIVED JULY 10, 1997
MANUSCRIPT ACCEPTED MARCH 4, 1998
PAPER HANDLED BY J. WILLIAM CAREY